Solid State Sciences 114 (2021) 106528

Contents lists available at ScienceDirect

Solid State Sciences

journal homepage: http://www.elsevier.com/locate/ssscie

Structural and spectroscopic investigation of a novel orange-red $Ca_9Bi(PO_4)_7$:Sm^{3+} nano-scaled phosphor

Anju Siwach, Dinesh Kumar *

Department of Chemistry, Deenbandhu Chhotu Ram University of Science & Technology, Murthal, Sonepat, 131039, India

ARTICLE INFO

Keywords:
Photoluminescence
Rietveld refinement
Scherrer's equation
Dexter's theory
Concentration quenching
CIE color Co-ordinate

ABSTRACT

A series of Sm^{3+} activated $Ca_9Bi(PO_4)_7$ novel tunable orange-red-emitting nanophosphors with an intense emission band at 600 nm were synthesized using the solution combustion method. The crystal structure, phase purity, structural parameters, optical band gap values, photoluminescence (PL) behavior, energy transfer, quantum efficiencies, lifetime values, and CIE chromaticity index of $Ca_9Bi_{(1-x)}Sm_x(PO_4)_7$ white powdered samples were consistently analyzed. Rietveld refinement of $Ca_9Bi_{0.88}(PO_4)_7$:012Sm^{3+} sample resulted into a trigonal crystal structure of sample having space group R3*c*(161) with refinement converged to R_p = 7.62%, R_{wp} = 12.01%, and $\chi^2 = 2.08$. Meanwhile, the average crystallite size for $Ca_9Bi_{0.88}Sm_{0.12}(PO_4)_7$ system was found out to be nearly 60 nm which was also supported by TEM images. The energy band-gap (E_g) value of $Ca_9Bi_{0.88}Sm_{0.12}(PO_4)_7$ was estimated to be 4.07 eV and the critical distance between Sm^{3+} ions was calculated to be 21.09 Å. The optimum concentration of dopant Sm^{3+} ions in $Ca_9Bi(PO_4)_7$ sample was ascertained to be 12 mol% and as per Dexter's theory and Huang study, the mechanism behind energy transfer between Sm^{3+} ions was concluded as dipole-dipole interactions. Under excitation at 403 nm, these nanophosphors exhibited three bands in the PL emission spectrum peaking at 562 nm, 600 nm, and 646 nm corresponding to $^4G_{5/2} \rightarrow {}^6H_J$ transitions (J = 5/2, 7/2, and 9/2, respectively). A decrease in lifetime values from 1.95 ms to 1.39 ms was observed with increased Sm^{3+} ions concentration. Upon employing Auzel's fitting function, radiative lifetime; non-radiative rates, and quantum efficiencies for as-synthesized nanophosphors were measured. The CIE color coordinate of $Ca_9Bi_{0.88}(PO_4)_7$:0.12Sm^{3+} was found to be (0.435, 0.354) and the corresponding quantum efficiency was estimated at 70.6%. The results obtained from our current study indicate that $Ca_9Bi(PO_4)_7$ doped with Sm^{3+} ions can have applicability as a promising orange-red-emitting nanophosphor for near-UV energized WLEDs.

1. Introduction

Over some past years, rare-earth (RE) ions activated inorganic luminescent materials i.e. nanophosphors have gained so much of the consideration of researchers. The WLED (White Light Emitting Diode) as a lighting device of the new era has emerged out as a need to conserve energy and the invention of certain technologies that can efficiently utilize the available sources of energy is a matter of keen interest of the scientists [1–3]. Though the discovery of nanophosphors is nearly 25 years old [4] but still various research pertaining to the development of phosphor-converted WLEDs (pc-WLEDs) with remarkable properties like outstanding luminescence performance, highly heat-resistant, eco-friendly, long life, compactly sized, etc is prevailing nowadays up to a large extent [4–10].

Presently, most of the commercially available typical WLEDs are synthesized by combining In, GaN blue LED chip with a yellow emitting $Y_3Al_5O_{12}$:Ce^{3+} phosphor. However, owing to the lack of red-component of light in the emission spectra, these pc-WLEDs, unfortunately, exhibit inadequate CRI (color rendering index) and high CCT (color correlated temperature) which further confine their applicability up to a certain limit [11–14]. For the purpose of obtaining white light emission for LEDs, an alternate yet effective method involving fabrication of UV-LED chip by coating with tricolor red, green and blue (RGB) phosphors has been adopted to overcome the drawbacks of the earlier method [15–19]. Although, certain issues like complicated fabrication, color control, luminescence performance disparity, etc. have appeared in this method too which limits their usability in pc-WLEDs [20,21]. Consequently, it is crucial to develop a single-component white-light-emitting nanophosphor.

It is widely known that a nanophosphor is generally synthesized by

* Corresponding author.
E-mail address: dineshdalal8@rediffmail.com (D. Kumar).

https://doi.org/10.1016/j.solidstatesciences.2020.106528
Received 4 July 2020; Received in revised form 24 December 2020; Accepted 25 December 2020
Available online 30 January 2021

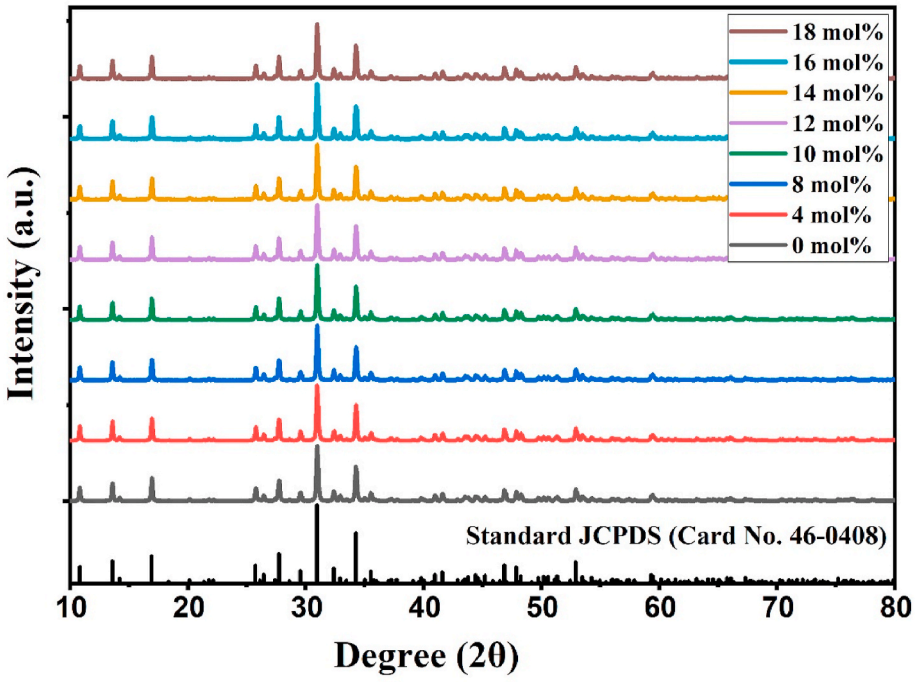

Fig. 1. The powder X-ray diffractograms of the pure host and $Ca_9Bi_{(1-x)}Sm_x(PO_4)_7$ (x = 0–0.18 mol) samples along with standard JCPDS Data of host $Ca_9Bi(PO_4)_7$.

incorporating a suitable RE metal ion (dopant) into a certain host lattice and the luminescent properties of that nanophosphor are majorly affected by both; the kind of dopant ion, and the crystalline structure of the host matrix [22]. The evident luminescence behavior shown by trivalent RE ions is due to the inter (4*f*-5*d*) and intra-configurational (4*f*-4*f*) electronic transitions. Out of various RE ions, the trivalent samarium (Sm^{3+}) ion is well worth selecting as a dopant ion for evaluating the luminescence performance of a nanophosphor because of its applicability in visible solid-state laser, high-density optical storage, and color displays [23]. Hence, Sm^{3+} is considered as a key activator ion for a wide range of inorganic hosts which give orange-red emission under near-ultraviolet (NUV) excitation owing to $^4G_{5/2} \rightarrow {}^6H_J$ (J = 5/2, 7/2, and 9/2) transitions [16,24–26].

Moreover, the selection of an excellent host plays an important role in attaining the desired results for pc-WLEDs. Being a significant kind of luminescent materials, phosphate compounds of type $M^I_9M^{II}(PO_4)_7$ (where M^I = divalent Ca, Ba, Sr ions and M^{II} = trivalent Gd, Y, Bi, Sc ions) are advantageous host materials for doping with RE ions, taking into account their high thermal, physical and chemical stability; stable crystal structure; easy and low-cost synthesis, and quite an appropriate phonon energy [3,22,27,28]. For the sake of our research report, we have selected $Ca_9Bi(PO_4)_7$ as an inorganic host compound that has been extensively used for doping with various RE ions to synthesize desirable luminescent nanomaterials. Some recent research reports on $Ca_9Bi(PO_4)_7$ doped with different rare-earth ions are available as $Ca_9Bi(PO_4)_7$:Dy^{3+} has been reported by Z.W. Zhang and co-workers [3]; $Ca_9Bi(PO_4)_7$:Eu^{3+} by Jyoti Dalal and co-workers [4]; also by Zhi-wei Zhang and co-workers [27]; $Ca_9Bi(PO_4)_7$:Eu^{2+},Dy^{3+} by Yonglei Jia and co-workers [28], and $Ca_9Bi(PO_4)_7$:Ce^{3+},Tb^{3+},Mn^{2+} by Kai Li and co-workers [29]. It is but obvious understood from previous research studies that $Ca_9Bi(PO_4)_7$ phosphate compound is a remarkable host matrix for rare-earth dopant ions. Nonetheless, so far no research report pertaining to the photoluminescence behavior of $Ca_9Bi(PO_4)_7$:Sm^{3+} has been published. To the best of our knowledge, the doping of Sm^{3+} in this host has been done for the first time.

Through our present research work, we report the synthesis of a series of novel, nanocrystalline, single-phase, orange-red-emitting $Ca_9Bi(PO_4)_7$:xSm^{3+} samples that have been performed first-ever via solution-combustion method. Rietveld refinement on $Ca_9Bi_{0.88}Sm_{0.12}(PO_4)_7$ nanophosphor system is carried out to examine the detailed crystal structural parameters. The energy band gap value (in eV) for the optimal concentration nanophosphor sample is determined using a diffuse reflectance spectrophotometer. Photoluminescence (PL) properties of $Ca_9Bi(PO_4)_7$:xSm^{3+} samples are investigated systematically through the PL excitation, emission spectra, and decay curve. The energy transfer mechanism which is occurring between Sm^{3+} ions is also analyzed. All these investigations are pointing towards the practicability of using orange-red-emitting $Ca_9Bi(PO_4)_7$:xSm^{3+} nanophosphors as pc-WLEDs under NUV excitation.

2. Synthesis and characterization

2.1. Sample preparation

In this work, the objective powder samples of RE (xSm^{3+}) doped $Ca_9Bi_{(1-x)}(PO_4)_7$ phosphors with the different chemical composition of activator (x = 0.04–0.18 mol) were synthesized by a very common yet an efficient technique involving combustion reaction route. Different analytical reagent grade chemicals like Calcium (II) nitrate tetrahydrate (98.9%, Central Drug House), Bismuth (III) nitrate pentahydrate (99%, Sigma-Aldrich), Samarium (III) nitrate hexahydrate (99.9%, Sigma-Aldrich), di-Ammonium hydrogen phosphate (99%, Sigma-Aldrich), and Urea (99–100%, Sigma-Aldrich) were purposed as constituent precursor materials. In this typical combustion synthesis process, firstly the uniform solution is prepared by mixing the stoichiometric amount of raw materials in double distilled water which was pre-sintered at 500 °C for about 20 min in the muffle furnace. Afterward, cooling to the room temperature, the sample was ground into the fine powdered form using agate mortar-pestle. The as-obtained homogenous powder sample was evenly put in the corundum crucible and then, sintered at 1200 °C for 3 h inside the furnace to obtain the white powdered phosphor as a final product. In a similar manner, the whole series of nanophosphors were synthesized, and thus collected for subsequent characterization. A chemical reaction representing the combustion synthesis of $Ca_9Bi_{0.88}Sm_{0.12}(PO_4)_7$ nanophosphor is given as follows:

$$75Ca(NO_3)_2.4H_2O + 7.33Bi(NO_3)_3.5H_2O + Sm(NO_3)_3.6H_2O + 58.33$$

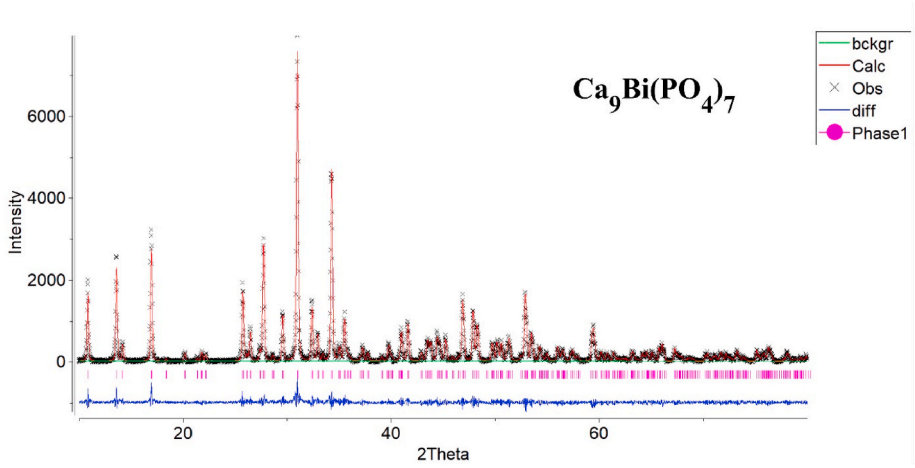

Fig. 2. Rietveld refinement pattern for the XRD data of $Ca_9Bi(PO_4)_7$ host sample where $R_{wp} = 15.62\%$, $R_p = 11.43\%$, and $\chi^2 = 2.52\%$.

$(NH_4)_2HPO_4 + 867.6NH_2.CO.NH_2 \rightarrow 8.33Ca_9Bi_{0.88}Sm_{0.12}(PO_4)_7 + 1013.5N_2 + 2340.5H_2 + 867.6CO_2$

2.2. Materials characterization

To analyze structure and phase purity, the powder diffraction profile of the series of as-prepared Sm^{3+} ions doped $Ca_9Bi(PO_4)_7$ phosphor samples were obtained in the 2θ range of $10^\circ - 80^\circ$ at a scan speed of 2° min^{-1} by using "Rigaku Ultima IV powder X-ray diffractometer" ($\lambda = 1.5405$ Å) which was maintained at a constant tube voltage (40 kV) and current (40 mV). In order to determine the lattice parameters and crystal structure refinement indices for $Ca_9Bi_{0.88}(PO_4)_7$:$0.12Sm^{3+}$, the Rietveld analysis using GSAS (General Structure Analysis System) package was applied to the graphical result obtained from the XRD pattern of this sample. DIAMOND software was then used to draw the crystal structure and co-ordination environment of different cations for the crystalline $Ca_9Bi_{0.88}Sm_{0.12}(PO_4)_7$ phosphor sample [8,30]. An instrument named "Technai- G^2 transmission electron microscope (TEM)" was used to examine the crystallite size and surface morphology of the best mol % Sm^{3+} ion activated $Ca_9Bi(PO_4)_7$ phosphor sample. The optical band gap value (in eV) represented in the diffuse reflectance spectrum of $Ca_9Bi_{0.88}Sm_{0.12}(PO_4)_7$ sample was determined with the help of "Shimadzu UV–Visible-3600 plus spectrophotometer", running at a wavelength scanning range 200–800 nm. The room-temperature measurements of photoluminescence excitation (recorded at wavelength range 200–500 nm), emission spectra (400–800 nm) and luminescence decay profiles for the whole series of $Ca_9Bi_{(1-x)}(PO_4)_7$:xSm^{3+} samples were performed by using "Hitachi F-7000 fluorescence spectrophotometer" which was accessorized with Xenon lamp (150 W) as a source of excitation. The "Commission International de I'Eclairage (CIE 1931) diagram" was used to indicate the color index (x,y) of all the as-obtained powdered samples upon employing MATLAB software on its PL emission spectral data [31].

3. Results and discussion

3.1. Phase and structural analysis

With the objective to examine the structure and phase purity of as-obtained crystalline phosphor samples, the XRD patterns of host $Ca_9Bi(PO_4)_7$ and trivalent samarium ions doped $Ca_9Bi(PO_4)_7$ phosphors with different doping concentrations of Sm^{3+} are compared with standard JCPDS (Card No. 46–0408) pattern of $Ca_9Bi(PO_4)_7$ [3]. Fig. 1 displays the X-ray diffraction profile of as-prepared samples of $Ca_9Bi_{(1-x)}Sm_x(PO_4)_7$ ($x = 0$, 0.04, 0.08, 0.10, 0.12, 0.14, 0.16, and 0.18 mol) and standard JCPDS data of $Ca_9Bi(PO_4)_7$ is presented as vertical lines in bottom of the same figure. The results achieved from XRD analysis substantiate that the synthesis of these compounds occurs in a single-phase crystal lattice as no detectable impurity peaks are found which further points out at the formation of solid solutions of whatsoever Bi^{3+}/Sm^{3+} ratio without any miscibility gap. This complies with Vegard's law, which foresees that "for the purpose of forming a solid solution of the cations of two compounds must have ionic radii within ±15% of each other" [27] and the co-ordination number 8 of our crystalline sample is supported well by the fact that Sm^{3+} and Bi^{3+} ions bear relatively similar ionic radii of 1.08 Å and 1.17 Å, respectively. Indeed, all the peaks in the XRD profile of phosphor samples coincide well with

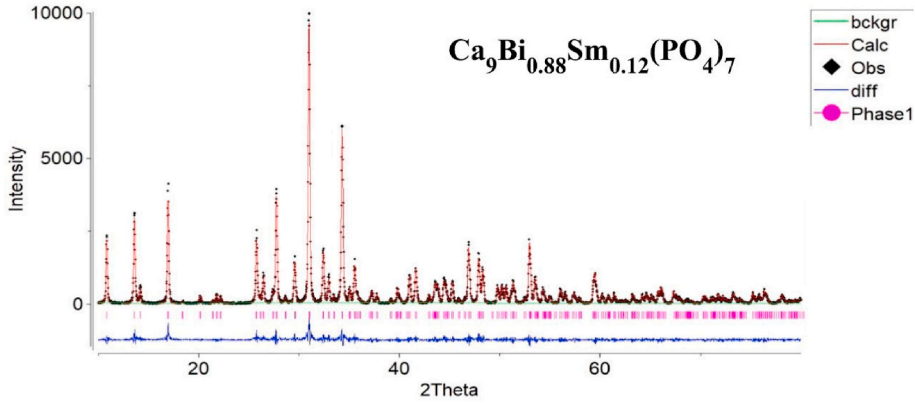

Fig. 3. Rietveld refinement pattern for the XRD data of $Ca_9Bi_{0.88}Sm_{0.12}(PO_4)_7$ nanophosphor sample where $R_{wp} = 12.01\%$, $R_p = 7.62\%$, and $\chi^2 = 2.08\%$.

Table 1
Comparison of lattice parameters of $Ca_9Bi_{(1-x)}Sm_x(PO_4)_7$ (x = 0–0.18 mol) nanophosphor series (trigonal crystal with R3*c* space group and Z = 6).

$Ca_9Bi_{(1-x)}Sm_x(PO_4)_7$	Formula Wt.	*a* (Å)	*c* (Å)	Volume (Å^3)	Density (g/cm^3)
$x = 0$	1232.80	10.4612(4)	37.4460(3)	3548.94	3.4607
$x = 0.04$	1230.48	10.4565(2)	37.4218(14)	3543.46	3.4595
$x = 0.08$	1228.16	10.4528(12)	37.4108(5)	3539.92	3.4580
$x = 0.10$	1227.00	10.4501(7)	37.3992(9)	3536.99	3.4560
$x = 0.12$	1226.61	10.4480(6)	37.3894(6)	3534.64	3.4549
$x = 0.14$	1224.68	10.4467(3)	37.3888(1)	3533.71	3.4527
$x = 0.16$	1223.52	10.4412(21)	37.3828(7)	3529.42	3.4536
$x = 0.18$	1222.36	10.4398(6)	37.3789(2)	3528.10	3.4516

that of the pure standard profile of $Ca_9Bi(PO_4)_7$ host. This further concludes that the introduction of trivalent samarium ions in different compositions into the host lattice does not result in any remarkable change in the parent crystal structure.

The Rietveld refinement of $Ca_9Bi(PO_4)_7$ and $Ca_9Bi_{0.88}Sm_{0.12}(PO_4)_7$ samples are shown in Fig. 2 and Fig. 3, respectively. Fig. 3 exhibits the observed (black diamond), calculated (red solid line), Bragg's lattice phase (pink bars), background (green line), and difference pattern (blue line at the bottom) of the XRD refinement pattern of $Ca_9Bi_{0.88}Sm_{0.12}(PO_4)_7$ phosphor sample. It is observed that the $Ca_9Bi_{0.88}Sm_{0.12}(PO_4)_7$ phosphor crystallizes in a trigonal lattice with space group R3*c*(161). Lattice parameters are ascertained to be $a = b =$ 10.4480 Å, c = 37.3894 Å, Z = 6, and V = 3534.64 Å^3 which is found to be quite similar to the host and other RE ions doped phosphors data reported in earlier research articles [4,28,29]. Furthermore, the crystallographic data details of $Ca_9Bi(PO_4)_7$ host and $Ca_9Bi_{1-x}Sm_x(PO_4)_7$ sample are listed in Table 1. Also, the final refinement for optimum luminescent composition converged with parameters R_{wp} = 12.01%, R_p = 7.62%, and χ^2 = 2.08% indicates a better fitting that gives low R-value. This better fitting further illustrates that there is no detectable impurity peak observed in the diffraction spectra. There are four cationic crystallographic sites from Ca(1) to Ca(4), out of which three non-centrosymmetric sites are octa-coordinated and shared between $Ca^{2+}/Bi^{3+}/Sm^{3+}$ ions; while the fourth centrosymmetric site is occupied by Ca^{2+} ions surrounded with six oxygen atoms in an octahedral manner.

To determine the average grain size (D) of crystalline powdered $Ca_9Bi_{0.88}Sm_{0.12}(PO_4)_7$ phosphor sample, a mathematical equation known as Scherrer's equation is used which is as follows [21,32]:

$$D = \frac{0.941\,\lambda}{\sqrt{\{\beta_o(2\theta) - \beta_{\,i}{}^2(2\theta)\}}.\,\mathrm{Cos}\theta} \quad (1)$$

As per equation (1), λ indicates the wavelength of X-ray Diffractometer whose value taken here is 0.154056 nm, θ indicates the diffraction angle, while $\beta_o(2\theta)$ = 0.00263 and $\beta_{Si}(2\theta)$ = 0.00084 represents full width at half maxima (FWHM in radian) for observed and standard silicon pattern, respectively. Upon solving the above equation for the series at 2θ = 31.046, the value of the particle size 60 nm is obtained. Furthermore, the TEM micrograph of $Ca_9Bi_{0.88}Sm_{0.12}(PO_4)_7$ system shown in Fig. 4 affirms the occurrence of somewhat spherical and agglomerated nanoparticles of nearly 40–70 nm size which is in congruence with the result obtained from the Scherrer's equation.

3.2. Band-gap energy measurement

The energy difference (in eV), also known as band-gap (E_g) value, between the valence and conduction band of Sm^{3+} doped $Ca_9Bi(PO_4)_7$ solid sample is determined by fitting its diffuse reflectance data (taken over an entire wavelength range of 200–800 nm) in the mathematical form of Kubelka- Munk (K-M) theory which is expressed as [33,34]:

$$[F(R_\infty)h\nu]^n = C(h\nu - E_g) \quad (2)$$

The above-mentioned equation gives a correlation between the coefficient of absorption $[F(R_\infty)h\nu]^n$ and the phonon energy i.e. $h\nu$ (in eV) which is displayed graphically in Fig. 5 for $Ca_9Bi_{0.88}(PO_4)_7$:0.12Sm^{3+} nanophosphor system. The inset of this figure shows the diffuse reflectance spectrum (DRS) which is a plot of reflectance vs wavelength of the sample. The value of n in the above equation can be 0.5, 1.5, 2, or 3 depending upon the allowed and forbidden transitions of direct or

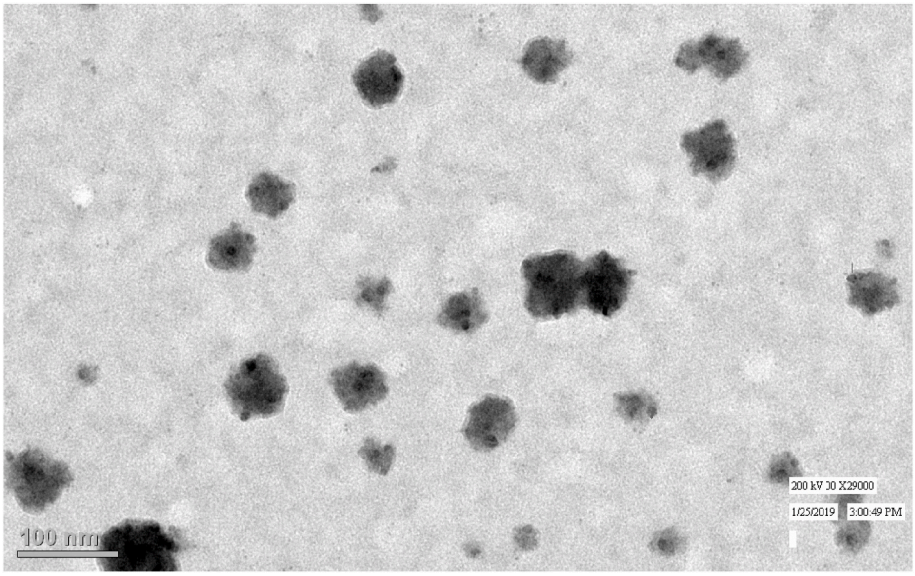

Fig. 4. A typical TEM picture of the powdered sample of $Ca_9Bi_{0.88}(PO_4)_7$:0.12Sm^{3+}.

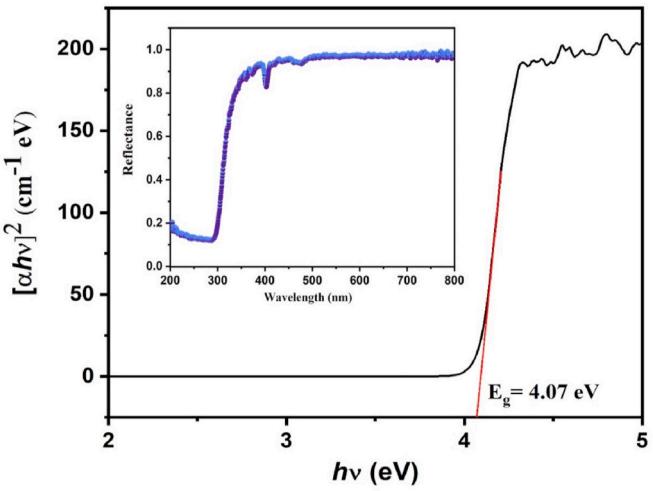

Fig. 5. A plot of $[\alpha h\nu]^2$ versus $h\nu$ for $Ca_9Bi_{(1-x)}Sm_x(PO_4)_7$ (x = 0.12) and extrapolation to determine the band gap energy using Kubelka-Munk equation. The inset shows the DRS of $Ca_9Bi_{0.88}Sm_{0.12}(PO_4)_7$ nanophosphor.

indirect types [11,35,36].

The above-mentioned K-M theory defines $F(R_\infty)$ as the ratio of absorption (K) and scattering (S) coefficient which can be written in a mathematical expression as [11,37,38]:

$$F(R_\infty) = \frac{(1-R_\infty)^2}{2R_\infty} = \frac{K}{S} \quad (3)$$

where, R_∞ is the reflectivity which represents the ratio of reflectivity of sample and the standard reflectivity. For the purpose to determine band-gap energy value (E_g) for $Ca_9Bi_{0.88}Sm_{0.12}(PO_4)_7$ system, extrapolation of $[F(R_\infty)h\nu]^2$ function to zero yields 4.07 eV value of band-gap which is found to be low in comparison to the $E_g \sim 4.30$ eV for the inorganic host $Ca_9Bi(PO_4)_7$ matrix calculated in previous research works [4]. This can, therefore, be concluded that the introduction of dopant ions creates new energy states within the band-gap of the system which lowers the energy value of the band-gap in the doped phosphor sample.

3.3. Photoluminescence properties and energy transfer mechanism

The luminescence performance of Sm^{3+} ions in $Ca_9Bi(PO_4)_7$:Sm^{3+} nanophosphors is analyzed by photoluminescence excitation (PLE) and photoluminescence (PL) emission spectra. Fig. 6 represents the PLE spectra of a series $Ca_9Bi_{(1-x)}Sm_x(PO_4)_7$ nanophosphor samples (x = 4–18 mol%). In the triply ionized state, Samarium metal shows electronic configuration [Xe]$4f^5$ and has $^6H_{5/2}$ ground state energy level. The PL excitation spectrum of Sm^{3+} activated $Ca_9Bi_{(1-x)}(PO_4)_7$:xSm^{3+} phosphor samples present seven excitation bands in the near-UV and visible-blue regions monitored at an emission wavelength of 600 nm. The seven bands peaking at 345, 362, 375, 403, 416, 439, and 468 nm are associated with *f-f* electronic transitions of Sm^{3+} ion from ground state $^6H_{5/2}$ to excited states $^4K_{17/2}$, $^4H_{7/2}$, $^6P_{7/2}$, $^4F_{7/2}$, $^6P_{5/2}$, $^4G_{9/2}$, and $^4I_{11/2}$, respectively [22]. By integrated peak area analysis, the peak centered at 403 nm corresponding to $^6H_{5/2} \rightarrow {}^4F_{7/2}$ has the highest intensity, hence 403 nm wavelength of excitation is selected to record emission spectra of our as-synthesized samples.

Fig. 7 portrays the photoluminescence emission spectra (noticed at an excitation wavelength of 403 nm) of as-obtained, differently doped $Ca_9Bi_{(1-x)}Sm_x(PO_4)_7$ nanophosphor samples where x is the concentration of trivalent samarium ions varying from 4 mol% to 18 mol%. The spectrum comprises of three major emission peaks occurring at 562 nm ($^4G_{5/2} \rightarrow {}^6H_{5/2}$, magnetic dipole allowed transition), 600 nm ($^4G_{5/2} \rightarrow {}^6H_{7/2}$, partially electric and partially magnetic dipole allowed transition), and 646 nm ($^4G_{5/2} \rightarrow {}^6H_{9/2}$, electric dipole allowed transition), out of which peak corresponding to $^4G_{5/2} \rightarrow {}^6H_{7/2}$ transition is the strongest of all [16]. Lastly, it can be concluded from the PL spectra of $Ca_9Bi_{(1-x)}Sm_x(PO_4)_7$ nanophosphor systems that when the samples are irradiated by UV or near-UV light, they show characteristic orange-red luminescence due to the most intense emission at 600 nm. A complete and combined photoluminescence spectrum over an entire wavelength range of 200–800 nm for $Ca_9Bi_{0.88}Sm_{0.12}(PO_4)_7$ nanophosphor showing all the excitation and emission peaks, and their corresponding *f-f* transitions are depicted well in Fig. 8.

In order to explain the process of energy transfer occurring in Sm^{3+} ions, a schematic energy level plot is represented in Fig. 9 which can be explained as firstly, the electrons are excited to various energy states from the ground $^6H_{5/2}$ level of Sm^{3+} ions that correspond to the seven excitation transitions from 345 nm to 468 nm. The excited electrons then

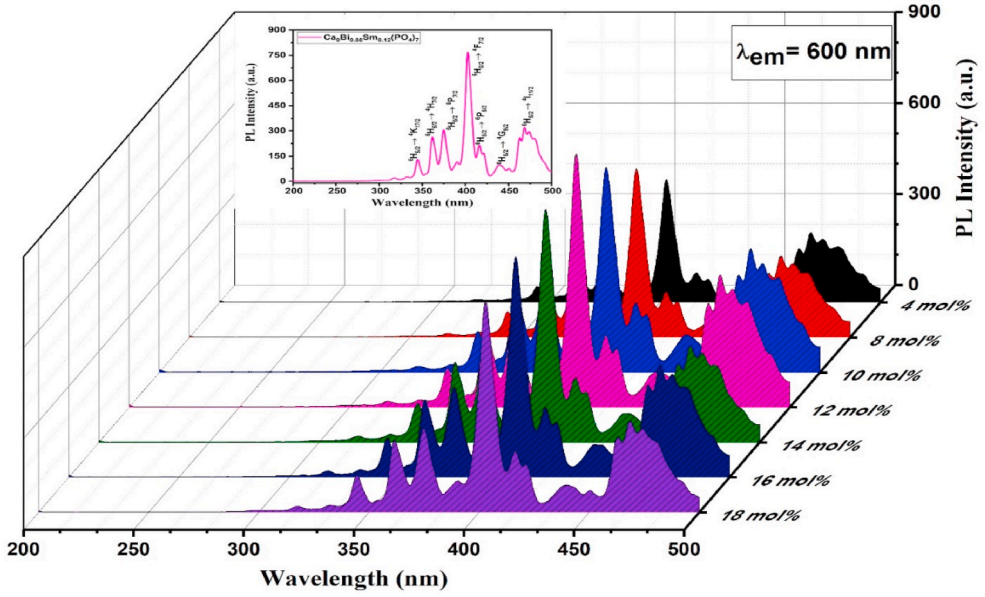

Fig. 6. The photoluminescence excitation (PLE) of $Ca_9Bi_{(1-x)}Sm_x(PO_4)_7$ nanophosphors (monitored at λ_{em} = 600 nm) with x = 0.04 to 0.18 as a function of Sm^{3+} ion concentrations. The inset at the top shows the PLE spectra of $Ca_9Bi_{0.88}Sm_{0.12}(PO_4)_7$ along with various possible transitions.

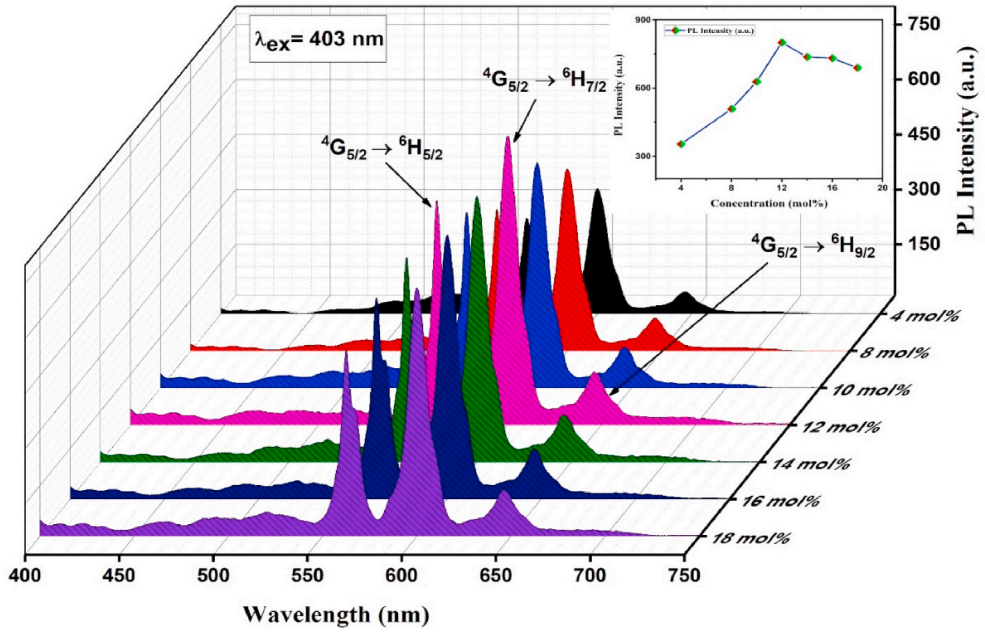

Fig. 7. Variation of photoluminescence intensities of $Ca_9Bi(PO_4)_7$ with different concentrations of Sm^{3+} ion in PL emission spectra observed at $\lambda_{ex} = 403$ nm. The inset is showing the effect of concentration on PL intensities of $Ca_9Bi_{(1-x)}Sm_x(PO_4)_7$ nanophosphors ($x = 0.04–0.18$).

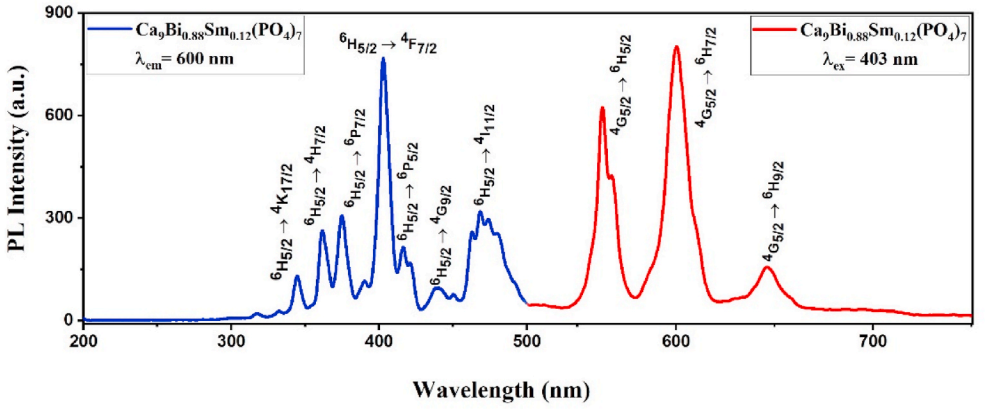

Fig. 8. A combined PL excitation (at $\lambda_{em} = 600$ nm) and emission (at $\lambda_{ex} = 403$ nm) spectra of $Ca_9Bi_{0.88}Sm_{0.12}(PO_4)_7$ nanophosphor.

relax non-radiatively to the low-lying $^4G_{5/2}$ energy state, as a result of which this level becomes the most populated one. Hence, the radiative emission to the various levels now takes place from $^4G_{5/2}$ emitting state to the ^6H_J (J = 5/2, 7/2, and 9/2) energy states giving rise to characteristic emission peaks of Sm^{3+} ions at 562, 600, and 646 nm.

Meanwhile, the episode of concentration quenching is also observed that can easily be seen from the inset of Fig. 7 which is displaying the relative intensity of emission as a function of Sm^{3+} ion concentrations (x = 0.04–0.18 mol). It is evident from the plot that the intensities of emission at 600 nm of $Ca_9Bi_{(1-x)}Sm_x(PO_4)_7$ (x = 0.04, 0.08, 0.10, 0.12, 0.14, 0.16, and 0.18 mol) series of nanophosphors increase with the increase in the concentration of dopant Sm^{3+} ions up to 0.12 mol which is considered as the best mol% concentration and then, the intensity declines with further increase in Sm^{3+} concentration. This may be attributed to the concentration quenching of Sm^{3+} ions.

Usually, the phenomenon of concentration quenching is primarily induced by energy transfers of non-radiative nature occurring among dopant trivalent samarium ions and according to Dexter's theory, there are three mechanisms corresponding to such energy transfers; namely exchange interactions, energy re-absorptions, and electric multipole-multipole interactions [39,40]. So, in a way to predict the type of energy transfer mechanism being followed in $Ca_9Bi_{0.88}(PO_4)_7$:0.12Sm^{3+} nanophosphor, the value of critical energy transfer distance (R_c) has to be calculated which can be easily done by adopting Blasse's equation [41]. The relationship given by Blasse to evaluate R_c by the critical concentration of Sm^{3+} ions is given as below [39,42]:

$$R_c = 2\left[\frac{3V}{4\ \pi\ x_c N}\right]^{1/3} \quad (4)$$

where V represents the unit cell volume, x_c refers to the critical concentration, and N is the number of formula units per unit cell. For $Ca_9Bi_{0.88}(PO_4)_7$:0.12Sm^{3+} trigonal crystal system, putting V = 3534.64 $Å^3$, $x_c = 0.12$, and N = 6 in above mentioned equation (4), the value of R_c of Sm^{3+} is estimated to be 21.09 Å. Since the result of R_c in $Ca_9Bi_{0.88}Sm_{0.12}(PO_4)_7$ system is far more than 5 Å, the possibility of an exchange interaction type of mechanism is ruled out [28]. Also, the energy re-absorption mechanism is effective only when there is a spectral overlap between emission and excitation bands which doesn't occur in our system case [32,43]. Consequently, the energy transfer (cross--relaxation) in $Ca_9Bi_{0.88}Sm_{0.12}(PO_4)_7$ nanophosphor is likely to happen

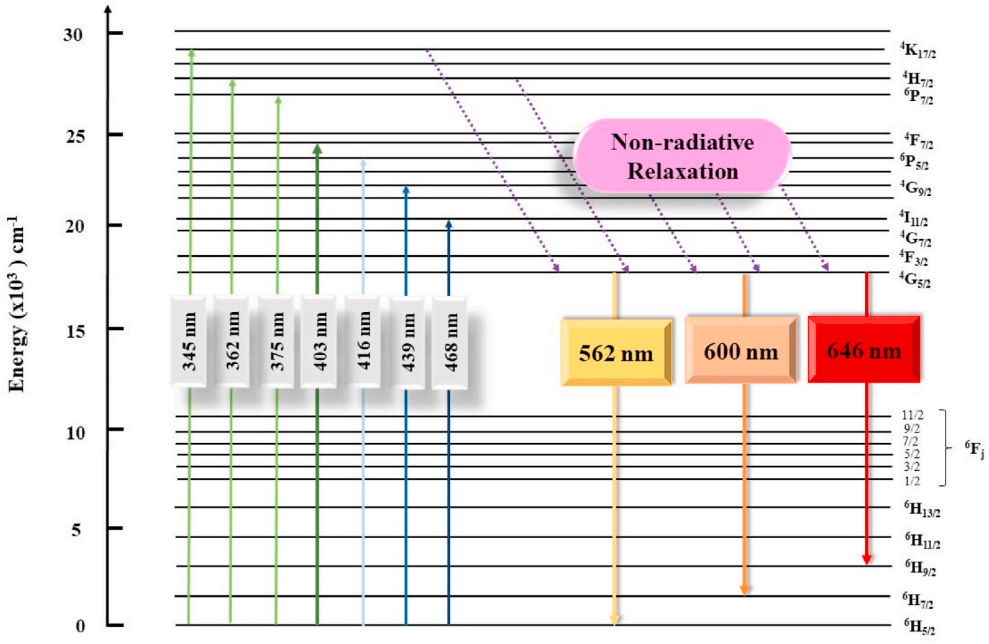

Fig. 9. A schematic energy level plot displaying all the *f-f* transitions observed in Sm^{3+} doped $Ca_9Bi(PO_4)_7$ phosphors.

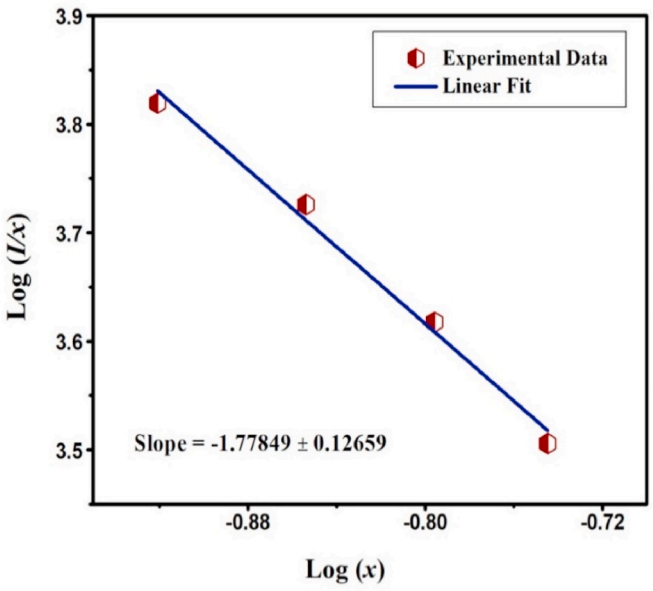

Fig. 10. Plot illustrating the dependence of I/x on x on a logarithmic scale in $Ca_9Bi(PO_4)_7$:$x$$Sm^{3+}$ nanophosphors where x is taken to be 0.12, 0.14, 0.16 and 0.18.

via electric multipolar interactions.

Huang and co-workers also developed the correlation between the photoluminescence emission intensity and the doping concentration after best-emission concentration as [44,45]:

$$\log\left(\frac{I}{x}\right) = \log(f) - \left(\frac{Q}{3}\right)\log x \tag{5}$$

where, x be the activator ion (Sm^{3+}) concentration, I is the integral intensity of emission spectra, I/x is emission intensity per activator ion, f is a concentration-independent constant, Q is a measure of electric multipolar interaction, as the values of Q = 6, 8 or 10 represent dipole-dipole (d-d), dipole-quadrupole (d-q) or quadrupole-quadrupole (q-q) interactions, respectively [46]. By plotting $\log\left(\frac{I}{x}\right)$ vs $\log x$, a straight-line graph having a negative slope is obtained, and the slope value i.e. −1.778 as depicted in Fig. 10 is just equivalent to the (−Q/3) in the above-mentioned equation (5). Hence, the resulting value of Q comes out to be 5.33 (approximately equal to 6) which indicates that the main energy transfer mechanism supporting concentration quenching of Sm^{3+} ion-doped $Ca_9Bi(PO_4)_7$ phosphors is d-d (dipole-dipole) interactions.

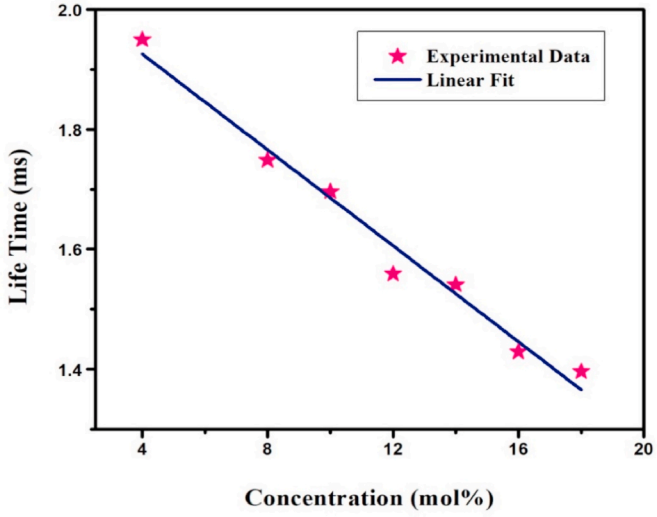

Fig. 11. Photoluminescence decay profile of $^4G_{5/2}$ state in Sm^{3+} doped $Ca_9Bi(PO_4)_7$ nanophosphor samples with different concentrations when excited at 403 nm.

3.4. Photoluminescence decay curves

To further analyze the energy transfer behavior, the decay profile showing the luminescence lifetimes of $Ca_9Bi_{(1-x)}(PO_4)_7$:$x$$Sm^{3+}$ (where x departs from 4 to 18 mol%) nanocrystalline solid samples are examined

Table 2
The lifetime decay values, non-radiative relaxation rates and quantum efficiencies of $^4G_{5/2}$ emitting ground state in $Ca_9Bi_{(1-x)}Sm_x(PO_4)_7$ (x = 0.04–0.18 mol) nanophosphors.

S. No.	Sm^{3+} concentrations (mol %)	Average lifetime (ms)	Non-radiative rates (s^{-1})	Quantum efficiency (%)
1.	4	1.95	60.3	88.2
2.	8	1.75	118.9	79.2
3.	10	1.69	139.2	76.5
4.	12	1.56	188.5	70.6
5.	14	1.54	196.8	69.7
6.	16	1.42	251.7	64.3
7.	18	1.39	266.9	62.9

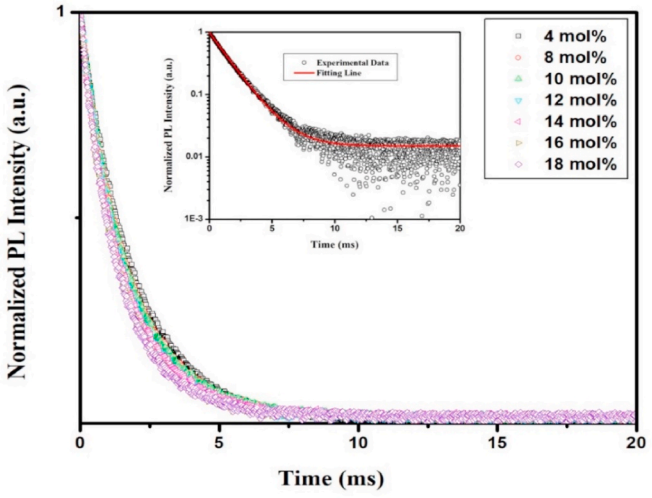

Fig. 12. Variation of average lifetime values as a function of concentration of Sm^{3+} ions in $Ca_9Bi_{(1-x)}Sm_x(PO_4)_7$ (x = 4–18 mol%) nanophosphors.

for $^4G_{5/2} \rightarrow {}^6H_{7/2}$ emission transition observed at 600 nm at λ_{ex} = 403 nm. The photoluminescence decay curves are shown in Fig. 11 and these can be fitted well with a single-order exponential decay mode and the experimental fitting data for the best mol% nanophosphor sample $Ca_9Bi_{0.88}Sm_{0.12}(PO_4)_7$ is displayed in the inset of the same figure. The first-order exponential decay equation can be expressed into a mathematical form as [4,47–49]:

$$I(t) = I_0 + A_1 \exp\left(\frac{-t}{\tau_1}\right) \tag{6}$$

Here, t indicates the time, I shows the luminescence intensity, A_1 is the constant, and τ_1 represents the fluorescence average decay time for the exponential component. The measured or average lifetime (τ) for first-order exponential decay is ascertained for a series of nanocrystalline samples $Ca_9Bi_{(1-x)}(PO_4)_7$: xSm^{3+} (x = 0.04, 0.08, 0.10, 0.12, 0.14, 0.16, and 0.18 mol), corresponding to the $^4G_{5/2}$ energy state of trivalent samarium ions, the average lifetime values are found out to be 1.95, 1.75, 1.69, 1.56, 1.54, 1.42, and 1.39 ms, respectively that are enlisted in Table 2. The as-obtained result points out at the relatively high emission efficacy because of the relatively short average decay values of the excited state of Sm^{3+} ions [22].

The variation of measured lifetimes as a function of different doping concentrations (x) of Sm^{3+} in $Ca_9Bi(PO_4)_7$ host lattice is depicted in Fig. 12. It is noticed well from both Table 2 and Fig. 12 that as the concentration of dopant ions increase from 4 mol% to 18 mol%, a linear drop-off in the average lifetime values from 1.95 ms to 1.39 ms is observed which may be attributed to the non-radiative energy transfer that takes place between different energy states of the dopant ions [32].

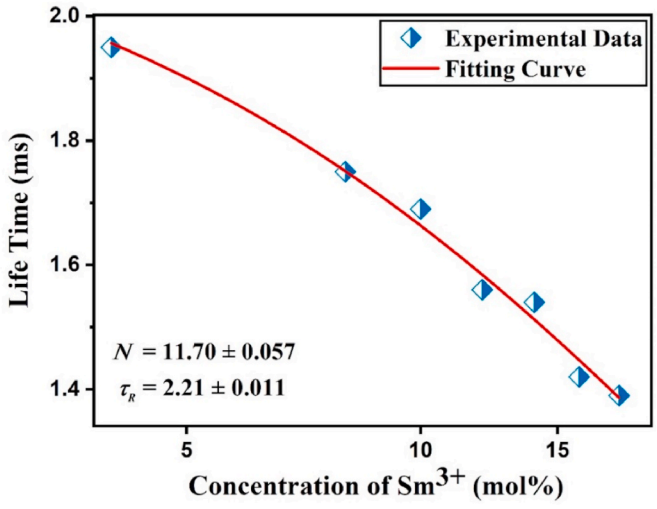

Fig. 13. Plot showing the dependence of lifetime value of $^4G_{5/2}$ state on different amount of dopant Sm^{3+} ions using Auzel's fitting function.

In addition to the values of fluorescence lifetime obtained (in ms) for $Ca_9Bi_{(1-x)}(PO_4)_7$: xSm^{3+} nanophosphor series, the relationship showing the dependence of as-obtained lifetime values on doping concentration of Sm^{3+} ions for self-generated quenching process is explained by Auzel's model which can be expressed mathematically as [32,33]:

$$\tau(c) = \frac{\tau_R}{1 + \left(\frac{c}{c_0}\right) e^{-N/3}} \tag{7}$$

where $\tau(c)$ is the photoluminescence lifetime at concentration c, τ_R is the intrinsic radiative lifetime, c_o be the constant having the same dimension as that of concentration c, and N is the number of phonons generated in the quenching process of $^4G_{5/2}$ energy state of Sm^{3+} ions. The experimentally evaluated PL lifetime data are fitted with the help of equation (7), the results obtained are shown in Fig. 13. The solid red line shows the fitting curve and the blue diamond shape points display the experimental data. It is clearly seen in Fig. 13, fitting curve obtained from equation (7), fits well with the experimental data and in the fitting process, the value of N is determined as 11.70 which indicates the generation of approximately 12 phonons from the quenching of $^4G_{5/2}$ level through non-radiative relaxation. The value of is reconfirmed by the energy difference between $^4G_{5/2}$ to $^6H_{7/2}$ (~16000 cm^{-1} approx.) energy levels, which is nearly 13 times of the 1200 cm^{-1} (highest phonon energy of phosphate host) [4].

Also, based on Auzel's model, the intrinsic radiative lifetime (τ_R) for $^4G_{5/2}$ level is found out to be 2.21 ms which is further used to evaluate quantum efficiencies (φ) of low lying emitting $^4G_{5/2}$ state in $Ca_9Bi_{(1-x)}Sm_x(PO_4)_7$ (x = 0.04–0.18 mol) nanophosphor series using the equation given below [33,50]:

$$\varphi = \frac{\tau_o}{\tau_R} = \frac{A_R}{A_R + A_{nR}} \tag{8}$$

Here, τ_o and τ_R are the observed average and intrinsic lifetime values (in ms), respectively; while A_R and A_{nR} be the radiative and non-radiative rates of relaxation, respectively. Additionally, the non-radiative relaxation rate A_{nR} (in s^{-1}) can be calculated using τ_o and τ_R values in the expression mentioned as follows [33,36]:

$$\frac{1}{\tau_o} - \frac{1}{\tau_R} = A_{nR} \tag{9}$$

Therefore, the values of non-radiative rates and quantum efficiencies for the whole series of Sm^{3+} doped $Ca_9Bi(PO_4)_7$ nanophosphors are estimated and presented in Table 2. The significant value of the quantum

Table 3
CIE1931 color co-ordinates (x, y) for $Ca_9Bi_{(1-x)}Sm_x(PO_4)_7$ (x = 0.04–0.18 mol) nanophosphors.

S. No.	Sm^{3+} concentrations (mol%)	CIE Color co-ordinates (x, y)
1.	4	(0.4137, 0.3924)
2.	8	(0.4268, 0.3683)
3.	10	(0.4379, 0.3773)
4.	12	(0.4347, 0.3536)
5.	14	(0.4451, 0.3826)
6.	16	(0.4453, 0.3758)
7.	18	(0.4300, 0.3707)

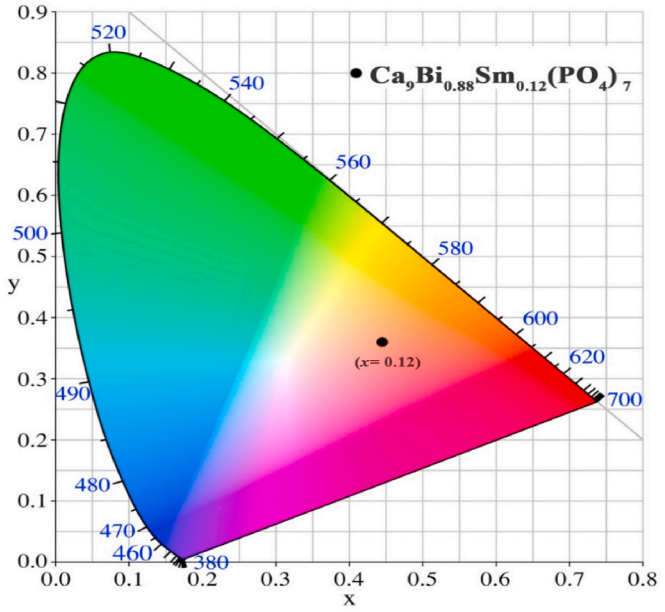

Fig. 14. CIE 1931 color co-ordinates for $Ca_9Bi(PO_4)_7$:$0.12Sm^{3+}$ activated at 403 nm. (For interpretation of the references to color in this figure legend, the reader is referred to the Web version of this article.)

efficiency (~71%) for the best mol% doped composition of our nanophosphor sample $Ca_9Bi_{0.88}Sm_{0.12}(PO_4)_7$ points out its efficient applicability in solid-state lighting (SSL) devices and displays.

3.5. CIE color coordinates

CIE chromaticity index (x,y) for the series of nanocrystalline samples $Ca_9Bi_{(1-x)}Sm_x(PO_4)_7$ (x = 0.04–0.18 mol) are calculated by adopting standard procedure under excitation of 403 nm which are listed in Table 3. In order to examine the luminescence color of our synthesized series of samples, MATLAB software and CIE1931 diagram are used to evaluate and plot the color coordinates [31,36]. Fig. 14 portrays the (x, y) values of the best mol% composition ($Ca_9Bi_{0.88}Sm_{0.12}(PO_4)_7$ phosphor) sample with solid black dot and chromaticity index of $Ca_9Bi_{0.88}Sm_{0.12}(PO_4)_7$ sample lie in the orange-red region. It can be concluded that under UV or near-UV excitation, $Ca_9Bi_{0.88}Sm_{0.12}(PO_4)_7$ nanophosphor sample shows bright orange-red luminescence which lastly encourages its usability in advance display and lighting devices.

4. Conclusion

Concisely, a series of single-phase nanocrystalline Sm^{3+} activated orange-red emitting $Ca_9Bi(PO_4)_7$:Sm^{3+} white powdered samples are productively synthesized by solution combustion route at 1200 °C. Rietveld analysis of our optimum concentration sample $Ca_9Bi_{0.88}Sm_{0.12}(PO_4)_7$ revealed the occurrence of different cations into a trigonal crystal lattice structure with R3c(161) space geometry. The energy band gap value of $Ca_9Bi_{0.88}(PO_4)_7$:$0.12Sm^{3+}$ nanocrystalline system (4.07 eV) is found out to be less than that of the host $Ca_9Bi(PO_4)_7$ system (4.30 eV). The PL emission spectral report disclosed the presence of three emission bands out of which the most intense one is appearing at 600 nm under near-UV excitation of 403 nm. Using Dexter's theory and Huang report, the energy transfer mechanism explaining the concentration quenching phenomenon has been established to be dipole-dipole interactions. The observed decay time (1.56 ms), non-radiative rate (188.5 s^{-1}), quantum efficiency (~71%), and CIE color coordinates (0.4347, 0.3536) of $Ca_9Bi_{0.88}Sm_{0.12}(PO_4)_7$ sample conclude that this novel orange-red nanophosphor has superior luminescence functioning and hence, $Ca_9Bi_{0.88}Sm_{0.12}(PO_4)_7$ nanophosphor can be significantly used as promising materials in LEDs or other display devices.

Author aggrement

We declare that this manuscript is original, has not been published before and is not being considered for publication elsewhere. We confirm that the manuscript has been read and approved by all co-authors and that there are no other persons who satisfied the criteria for authorship but are not listed. We further confirm that the order of authors listed in the manuscript has been approved by all of us. I understand that the Corresponding Author is the sole contact for the Editorial process. I am responsible for communicating with the other authors about progress, submissions of revisions and final approval of proofs.

Declaration of competing interest

The authors declare that they have no known competing financial interests or personal relationships that could have appeared to influence the work reported in this paper.

References

[1] G. Zhu, Z. Ci, Y. Shi, M. Que, Q. Wang, Y. Wang, Synthesis, crystal structure and luminescence characteristics of a novel red phosphor Ca19Mg2(PO4)14:Eu3+ for light emitting diodes and field emission displays, J. Mater. Chem. C 1 (2013) 5960–5969.
[2] Z. Zhou, N. Wang, N. Zhou, Z. He, S. Liu, Y. Liu, Z. Tian, Z. Mao, H.T. Hintzen, High color purity single-phased full colour emitting white LED phosphor Sr2V2O7 : Eu3+, J. Phys. D Appl. Phys. 46 (2013), 035104.
[3] Z.W. Zhang, A.J. Song, Y. Hue, H. Zhong, X.Y. Zhang, M.Z. Ma, R.P. Liu, White light emission from $Ca_9Bi(PO_4)_7$:Dy^{3+} single-phase phosphors for light-emitting diodes, J. Alloys Compd. 650 (2015) 410–414.
[4] J. Dalal, M. Dalal, S. Devi, A. Hooda, A. Khatkar, V.B. Taxak, S.P. Khatkar, Radiative and non-radiative characteristics of $Ca_9Bi(PO_4)_7$: Eu^{3+} nano-phosphor for solid state lighting devices, J. Lumin. 216 (2019) 116697.
[5] J. Zhou, Z. Xia, M. Yang, K. Shen, High efficiency blue-emitting phosphor: Ce3+-doped Ca5.45Li3.55(SiO4)3O0.45F1.55 for near UV-pumped light-emitting diodes, J. Mater. Chem. 22 (2012) 21935–21941.
[6] Z.W. Zhang, L. Liu, R. Liu, X.-y. Zhang, X.-g. Peng, C.-h. Wang, D.-j. Wang, High-brightness Eu3+-doped Ca9Gd(PO4)7 red phosphor for NUV light-emitting diodes application, Mater. Lett. 167 (2016) 250–253.
[7] X. Zhang, L. Zhou, Q. Pang, M. Gong, Synthesis, photoluminescence, and Judd–Ofelt analysis of red LiGd5P2O13 : Eu3+ phosphors for white LEDs, RSC Adv. 5 (2015) 54622–54628.
[8] R. Yu, H. Mi Noh, B. Kee Moon, B. Chun Choi, J. Hyun Jeong, H. Sueb Lee, K. Jang, S. Soo Yi, Photoluminescence characteristics of Sm3+-doped Ba2CaWO6 as new orange–red emitting phosphors, J. Lumin. 152 (2014) 133–137.
[9] Q. Sun, B. Li, S. Wang, H. Guo, X. Huang, Photoluminescence properties of a novel rare-earth-free red-emitting Ca3Y(AlO)3(BO3)4:Mn4+ phosphor for white LEDs application, J. Mater. Sci. Mater. Electron. 29 (2018) 12972–12977.
[10] L. Sun, H. Guo, J. Liang, B. Li, X. Huang, Ca3Lu(GaO)3(BO3)4:Eu 3+ : a novel high-brightness and thermal-stable red-emitting phosphor for white LEDs, J. Lumin. 202 (2018) 403–408.
[11] L. Yang, Z. Mu, S. Zhang, Q. Wang, D. Zhu, Y. Zhao, D. Luo, Q. Zhang, F. Wu, Dy3+ Doped Ca9Gd(PO4)7: a novel single-phase full-color emitting phosphor, J. Mater. Sci. Mater. Electron. 29 (2018) 6548–6555.
[12] H. Xu, L. Wang, D. Qu, Z. Si, J. Shi, Structure and photoluminescence properties of novel Sr6Ca4(PO4)6F2:Re (Re = Eu2+, Mn2+) phosphors with energy transfer for white-emitting LEDs, RSC Adv. 7 (2017) 41282–41288.
[13] D. Wu, W. Xiao, L. Zhang, X. Zhang, Z. Hao, G.-H. Pan, Y. Luo, J. Zhang, Simultaneously tuning the emission color and improving thermal stability via

energy transfer in apatite-type phosphors, J. Mater. Chem. C 5 (2017) 11910–11919.
[14] L.L. Wang, Q.-L. Wang, X.-Y. Xu, J.-Z. Li, L.-B. Gao, W.-K. Kang, J.-S. Shi, J. Wang, Energy transfer from Bi3+ to Eu3+ triggers exceptional long-wavelength excitation band in ZnWO4:Bi3+, Eu3+ phosphors, J. Mater. Chem. C 1 (2013) 8033–8040.
[15] X. Wang, Z. Zhao, Q. Wu, Y. Li, C. Wang, A. Mao, Y. Wang, Synthesis, structure, and luminescence properties of SrSiAl2O3N2:Eu(2+) phosphors for light-emitting devices and field emission displays, Dalton Trans. 44 (2015) 11057–11066.
[16] L. Wang, H.M. Noh, B.K. Moon, S.H. Park, K.H. Kim, J. Shi, J.H. Jeong, Dual-mode luminescence with broad near UV and blue excitation band from Sr2CaMoO6:Sm3+ phosphor for white LEDs, J. Phys. Chem. C 119 (2015) 15517–15525.
[17] G.G. Wang, X.-F. Wang, L.-W. Dong, Q. Yang, Synthesis and photoluminescence of green-emitting Ce3+,Tb3+ co-doped Al6Si2O13 phosphors with high thermal stability for white LEDs, RSC Adv. 6 (2016) 42770–42777.
[18] B. Li, Q. Sun, S. Wang, H. Guo, X. Huang, Ce3+ and Tb3+ doped Ca3Gd(AlO)3(BO3)4 phosphors: synthesis, tunable photoluminescence, thermal stability, and potential application in white LEDs, RSC Adv. 8 (2018) 9879–9886.
[19] Q. Liu, Y. Liu, Z. Yang, X. Li, Y. Han, UV-excited red-emitting phosphor Eu3+-activated Ca9Y(PO4)7,, Spectrochim. Acta Mol. Biomol. Spectrosc. 87 (2012) 190–193.
[20] H. Qian, J. Zhang, L. Yin, Crystal structure and optical properties of white light-emitting Y2WO6:Sm3+ phosphor with excellent color rendering, RSC Adv. 3 (2013) 9029–9034.
[21] H. Dahiya, M. Dalal, A. Siwach, M. Dahiya, D. Kumar, Cool white light emitting Ba5Zn4Y8O21:Dy3+ nanophosphors for single-phased WLEDs, J. Mater. Sci. Mater. Electron. 29 (2018) 20750–20758.
[22] Z. Yang, D. Xu, J. Sun, Y. Sun, H. Du, Characterization and luminescence properties of Sr3Gd(PO4)3:Sm3+ orange-red phosphor, Opt. Eng. 54 (10) (2015) 105102.
[23] M. Jayasimhadri, E.-J. Cho, K.-W. Jang, H.S. Lee, S.I. Kim, Spectroscopic properties and Judd–Ofelt analysis of Sm3+doped lead–germanate–tellurite glasses, J. Phys. D Appl. Phys. 41 (2008) 175101.
[24] Y. Shi, J. Shi, C. Dong, Luminescence characteristics and J-O analysis of BaWO 4 :3%Sm 3+ crystal for yellow phosphors, Ceram. Int. 43 (2017) 16356–16361.
[25] J. Wu, S. Shi, X. Wang, J. Li, R. Zong, W. Chen, Controlled synthesis and optimum luminescence of Sm3+-activated nano/submicroscale ceria particles by a facile approach, J. Mater. Chem. C 2 (2014) 2786–2792.
[26] R. Nagaraja, V. Pushpa Manjari, B. Sailaja, R.V.S.S.N. Ravikumar, A novel orange emitting Sm3+ ions doped NaCaAlPO4F3 phosphor: optical and luminescence properties, J. Mol. Struct. 1130 (2017) 96–102.
[27] Z.W. Zhang, L. Liu, S.-t. Song, J.-p. Zhang, D.-j. Wang, A novel red-emitting phosphor Ca9Bi(PO4)7:Eu3+ for near ultraviolet white light-emitting diodes, Curr. Appl. Phys. 15 (2015) 248–252.
[28] H.L. Yonglei Jia, Ran Zhao, Wenzhi Sun, Qiang Su, Ran Pang, Chengyu Li, Luminescence properties of a new bluish green long-lasting phosphorescence phosphor $Ca_9Bi(PO_4)_7$:Eu^{3+},Dy^{3+}, Opt. Mater. 36 (11) (2014) 1781–1786, https://doi.org/10.1016/j.optmat.2014.04.006.
[29] M.S. Kai Li, Yang Zhang, Jian Fan, Hongzhou Lian, Jun Lin, Photoluminescence properties of single-component white-emitting $Ca_9Bi(PO_4)_7$:Ce^{3+},Tb^{3+},Mn^{2+} phosphors for UV LEDs, J. Mater. Chem. C 3 (2015) 7096–7104.
[30] N. Zhang, C. Guo, J. Zheng, X. Su, J. Zhao, Synthesis, electronic structures, and luminescent properties of Eu3+ doped KGdTiO4, J. Mater. Chem. C 2 (2014) 3988–3994.
[31] H. Dahiya, M. Dalal, J. Dalal, V.B. Taxak, S.P. Khatkar, D. Kumar, Synthesis and luminescent properties of Tb3+ doped BaLa2ZnO5 nanoparticles, Mater. Res. Bull. 99 (2018) 86–92.
[32] J. Dalal, M. Dalal, S. Devi, R. Devi, A. Hooda, A. Khatkar, V.B. Taxak, S.P. Khatkar, Structural analysis and judd-ofelt parameterization of Ca9Gd(PO4)7:Eu3+ nanophosphor for solid-state illumination, J. Lumin. 210 (2019) 293–302.
[33] S. Devi, V.B. Taxak, S. Chahar, M. Dalal, J. Dalal, A. Hooda, A. Khatkar, R.K. Malik, S.P. Khatkar, Crystal chemistry and optical analysis of a novel perovskite type SrLa2Al2O7:Sm3+ nanophosphor for white LEDs, Ceram. Int. 45 (2019) 15571–15579.
[34] H. Dahiya, M. Dalal, A. Siwach, J. Dalal, V.B. Taxak, S.P. Khatkar, D. Kumar, A blue to green tunable Ba3GdP3O12:Tb3+ nanophosphor: structural and opto-electronic analysis, J. Mater. Sci. Mater. Electron. 31 (5) (2019) 3750–3758, https://doi.org/10.1007/s10854-019-02009-1.
[35] J. Zhao, C. Guo, T. Li, D. Song, X. Su, Near-infrared down-conversion and energy transfer mechanism in Yb(3+)-doped Ba2LaV3O11 phosphors, Phys. Chem. Chem. Phys. 17 (2015) 26330–26337.
[36] J. Dalal, M. Dalal, S. Devi, S. Chahar, A. Hooda, A. Khatkar, R.K. Malik, V.B. Taxak, S.P. Khatkar, Ba5Zn4Gd8O21:Tb3+ -Structural Characterization and the Judd-ofelt parameterization from emission spectra, Methods Appl. Fluoresc. 8 (3) (2019), https://doi.org/10.1088/2050-6120/ab33b6.
[37] M. Tian, P. Li, Z. Wang, X. Teng, Z. Li, J. Cheng, Y. Sun, C. Wang, Z. Yang, Synthesis, color-tunable emission, thermal stability, luminescence, and energy transfer of Sm3+ and Eu3+ single-doped M3Tb(BO3)3 (M = Sr and Ba) phosphors, CrystEngComm 18 (2016) 6934–6947.
[38] H. Dahia, A. Siwach, M. Dahiya, A. Singh, S. Nain, M. Dalal, S.P. Khatkar, V. B. Taxak, D. Kumar, Structural and Photo-luminescence examination of red emissive Eu^{3+}-doped nanophosphor synthesized via solution-combustion method, Chem. Phys. Lett. 754 (2020) 137657, https://doi.org/10.1016/j.cplett.2020.137657.
[39] Z. Yang, P. Liu, J. Li, Q. Yang, L. Lv, Y. Zhao, A novel yellow luminescent material Ba3Y(PO4)3:Eu2+, J. Alloys Compd. 578 (2013) 118–120.
[40] S. Chahar, R. Devi, M. Dalal, P. Boora, V.B. Taxak, S.P. Khatkar, Structural and photoluminescent analysis in Judd-Ofelt framework of color tunable SrGd2(1-x)Eu(2x)Al2 O7 nanophosphor for white light emitting materials, J. Lumin. 194 (2018) 271–278.
[41] J. Zhong, D. Chen, Y. Zhou, Z. Wan, M. Ding, W. Bai, Z. Ji, New Eu(3+)-activated perovskite La(0.5)Na(0.5)TiO3 phosphors in glass for warm white light emitting diodes, Dalton Trans. 45 (2016) 4762–4770.
[42] H. Dahiya, M. Dalal, A. Singh, A. Siwach, M. Dahiya, S. Nain, V.B. Taxak, S. P. Khatkar, D. Kumar, Spectroscopic Characteristics of Eu3+-Activated Ca9Y(PO4) 7 Nanophosphors in Judd-Ofelt Framework, Solid State Sci, 2020, p. 106341, https://doi.org/10.1016/j.solidstatesciences.2020.106341.
[43] M. Dalal, V.B. Taxak, J. Dalal, A. Khatkar, S. Chahar, R. Devi, S.P. Khatkar, Crystal structure and Judd-Ofelt properties of a novel color tunable blue-white-red Ba 5 Zn 4 Y 8 O 21 :Eu 3+ nanophosphor for near-ultraviolet based WLEDs, J. Alloys Compd. 698 (2017) 662–672.
[44] X. Huang, Preparation and luminescence characteristics of monazite Eu^{3+}:$LaPO_4$ nanocrystals in NH_4NO_3 molten salt, Opt. Mater. 50 (2015) 81–86.
[45] Y. Tian, B. Chen, B. Tian, R. Hua, J. Sun, L. Cheng, H. Zhong, X. Li, J. Zhang, Y. Zheng, T. Yu, L. Huang, Q. Meng, Concentration-dependent luminescence and energy transfer of flower-like $Y_2(MoO_4)_3$:Dy^{3+} phosphor, J. Alloys Compd. 509 (2011) 6096–6101.
[46] M. Dalal, J. Dalal, S. Chahar, H. Dahiya, S. Devi, P. Dhankhar, S. Kumar, V. B. Taxak, D. Kumar, S.P. Khatkar, A hybrid treatment of $Ba_2LaV_3O_{11}$:Eu^{3+} nanophosphor system: first-principal and experimental investigations into electronic, crystal and the optical structure, J. Alloys Compd. 805 (2019) 84–96.
[47] S. Chahar, M. Dalal, S. Singh, R. Devi, V.B. Taxak, S.P. Khatkar, Structural and photoluminescent elucidation of the efficient green emitting erbium doped BaY2ZnO5 nanophosphor for light emitting materials, J. Mater. Sci. Mater. Electron. (2017), https://doi.org/10.1007/s10854-017-8130-9.
[48] M. Dalal, V.B. Taxak, S. Chahar, A. Khatkar, S.P. Khatkar, A promising novel orange–red emitting SrZnV 2 O 7:Sm 3+ nanophosphor for phosphor-converted white LEDs with near-ultraviolet excitation, J. Phys. Chem. Solid. 89 (2016) 45–52.
[49] J. Chen, Y. Liu, L. Mei, H. Liu, M. Fang, Z. Huang, Crystal structure and temperature-dependent luminescence characteristics of KMg4(PO4)3:Eu(2+) phosphor for white light-emitting diodes, Sci. Rep. 5 (2015) 9673.
[50] S. Devi, M. Dalal, J. Dalal, A. Hooda, A. Khatkar, V.B. Taxak, Near-ultraviolet excited down-conversion Sm3+ doped Ba5Zn4Gd8O21 reddish-orange emitting nano-diametric rods for white LEDs, Ceram. Int. 45 (2019) 7397–7406.